Heteroaggregation Approach for Depositing Magnetite Nanoparticles onto Silica-Overcoated Gold Nanorods

As Published: 10.1021/ACS.CHEMMATER.7B03481

Publisher: American Chemical Society (ACS)

Persistent URL: https://hdl.handle.net/1721.1/134928

Version: Final published version: final published article, as it appeared in a journal, conference proceedings, or other formally published context

CHEMISTRY OF MATERIALS
Cite This: Chem. Mater. 2017, 29, 10362−10368
Article
pubs.acs.org/cm

Heteroaggregation Approach for Depositing Magnetite Nanoparticles onto Silica-Overcoated Gold Nanorods

Brian S. Chapman,[†] Wei-Chen Wu,[†] Qiaochu Li,[§] Niels Holten-Andersen,[§] and Joseph B. Tracy*[,†]

[†]Department of Materials Science and Engineering, North Carolina State University, Raleigh, North Carolina 27695, United States
[§]Department of Materials Science and Engineering, Massachusetts Institute of Technology, Cambridge, Massachusetts 02139, United States

Supporting Information

ABSTRACT: Hydrophobic, oleylamine-stabilized magnetite nanoparticles (Fe_3O_4 NPs) dispersed in hexanes can assemble into dense coatings on the surface of silica-overcoated gold nanorods (SiO_2-GNRs) dispersed in ethanol by mixing. In this nonaqueous heteroaggregation process, Fe_3O_4 NPs are destabilized when ethanol is added, resulting in core/satellite Fe_3O_4-SiO_2-GNRs within a few minutes. The composition of the solvent mixture allows tuning of the polarity and driving forces toward aggregation. At the optimal 2:1 volume ratio of hexanes:ethanol, heteroaggregation to form Fe_3O_4-SiO_2-GNRs occurs quickly, while avoiding homoaggregation of Fe_3O_4 NPs or SiO_2-GNRs. Fe_3O_4-SiO_2-GNRs retain the longitudinal surface plasmon resonance of the gold nanorod cores and are magnetically responsive and separable. The Fe_3O_4 NPs remain bound on the surface of the Fe_3O_4-SiO_2-GNRs during multiple cycles of magnetic extraction and redispersion. Oleylamine ligands on the Fe_3O_4 NPs render the Fe_3O_4-SiO_2-GNRs dispersible in nonpolar solvents. Functionalization of the outer Fe_3O_4 surface with poly(ethylene glycol) catechol (PEG-catechol) for PEGylation results in PEG-Fe_3O_4-SiO_2-GNRs that disperse in water. In comparison with seeded growth or use of molecular cross-linkers to form multifunctional nanoparticles, heteroaggregation approaches are potentially quite general, simple, and efficient. The ability to continuously adjust the solvent polarity is expected to allow tuning of the heteroaggregation process for many different types and sizes of NPs.

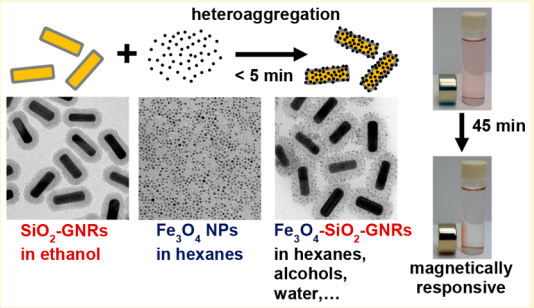

INTRODUCTION

Composite nanoparticles (NPs) integrate multiple NPs into single units and are usually formed through seeded growth of one kind of NP onto another or through cross-linker molecules. By combining different kinds of NPs into composite NPs, multifunctional NPs with novel optical, magnetic, electronic, or catalytic properties can be obtained.[1−3] There are several approaches for synthesizing composite NPs, which can have a variety of sizes and morphologies, such as clusters, dendrites, chains, and sheets.[4] For some applications, it is desirable to make compact composite NPs by maximizing the loading of functional NPs and minimizing the amount of cross-linker or inert matrix material. Here, we demonstrate a simple heteroaggregation approach for depositing coatings of magnetite (Fe_3O_4) NPs onto the surface of silica-overcoated gold nanorods (SiO_2-GNRs), resulting in Fe_3O_4-SiO_2-GNRs, which maintain the longitudinal surface plasmon resonance (LSPR) of gold nanorods and are magnetically responsive. Fe_3O_4-SiO_2-GNRs are of special interest for biomedical applications because they are composed of biocompatible building blocks and are potentially useful for multimodal imaging or photothermal therapy with magnetic targeting. Heteroaggregation is a simple and versatile approach for assembling core/satellite NPs that is potentially widely applicable.

A common method for synthesizing core/satellite and core/shell NPs is seeded growth, where one inorganic phase is grown directly onto another,[5−30] which strongly depends on the composition of both phases, and heterogeneous nucleation of the satellite phase onto the core can be difficult to control. Moreover, seeded growth can require significant modifications to methods initially developed for homogeneous nucleation of the satellite phase to suppress homogeneous nucleation and provide primarily or exclusively heterogeneous nucleation.[10] Control over the size and morphology of the shell of satellite NPs is also often limited. A related method is mixing precursors for different elements and driving phase segregation by heating, which depends on the thermodynamics of the specific system.[31]

Another approach is assembly of presynthesized satellite NPs onto the surface of the core NP. This can allow more precise control over formation of the satellite NPs, for which synthetic methods are often already well established. Assembly of satellite NPs onto a core NP can be achieved using covalent cross-linkers, noncovalent interactions, and steric effects. Noncovalent interactions include van der Waals interactions from strong electrostatic interactions to weaker dipolar interactions,

Received: August 16, 2017
Revised: November 4, 2017
Published: December 11, 2017

DOI: 10.1021/acs.chemmater.7b03481
Chem. Mater. 2017, 29, 10362−10368

biological interactions, and $\pi-\pi$ interactions.[32−38] Electrostatic attraction can be enhanced by selecting core and satellite NPs with opposite charges or by functionalizing them with opposite charges.[6,39,40] Covalent linkers are multifunctional molecules that can covalently bind to different types of NPs.[41−48] For steric effects to be significant, the coating on one type of NP must entrap the other type of NP or entangle its coating. Coatings designed for entrapment can be added in a step prior to assembly, or coating and assembly can be performed simultaneously, where the coating material serves as the mortar to hold NPs together. Common coating materials for entrapment include polymers[49] and inorganic oxides obtained through sol−gel chemistry, such as silica (SiO_2).[43,50−53]

Several types of core/satellite NPs with gold nanorod (GNR) cores have been formed through seeded growth,[6,27] van der Waals interactions,[6,54] multifunctional molecules,[55−59] biomolecules,[26,60,61] and polymers,[56] but these methods are often limited by low-density coatings or nonuniform coverage. The native cetyltrimethylammonium bromide (CTAB) coating on GNRs is a challenge for functionalization of GNRs because CTAB is difficult to displace in aqueous environments,[62] and CTAB-stabilized GNRs are prone to agglomeration in nonaqueous solvents that can facilitate removal of CTAB. The CTAB coating on GNRs can be destabilized by increasing the salt concentration, decreasing the CTAB concentration, or changing the solvent composition.[63] These limitations of the CTAB coating can be overcome by depositing SiO_2 shells onto the GNRs, which also provides colloidal stability in methanol and ethanol. Our heteroaggregation approach for forming core/satellite Fe_3O_4-SiO_2-GNRs is based on upon the ability of SiO_2-GNRs to disperse in alcohols.

Aggregation occurs when colloids, including NPs, are destabilized, form flocs, and settle out of solution. During aggregation processes, an energy barrier that would prevent aggregation is lowered or overcome, allowing aggregation to occur.[64,65] In homoaggregation, particles of the same type flocculate, while heteroaggregation describes flocculation of different kinds of particles. Aggregation is a stochastic process, where particles collide with one another, and if the attractive forces are strong enough or the barrier to aggregation is overcome, they remain bound together. In a binary particle system (A and B), three kinds of aggregation are possible, AA, BB, and AB. For stable colloidal suspensions, energy barriers prevent each kind of aggregation.[66,67] Manipulating the properties of the particles or their solvent environment can reduce or eliminate one or more of these barriers, thus driving aggregation.[68] If the barrier to AB aggregation is reduced or diminished while maintaining energy barriers for AA and BB aggregation, then heteroaggregation can occur selectively, without simultaneous homoaggregation.[69]

Multiple experimental levers are available for altering the energy barriers to aggregation. For example, removing stabilizing ligands from NPs can reduce the barrier to aggregation.[68] The solvent polarity can also be adjusted by adding a cosolvent with a different polarity that is miscible with the initial solvent, which can destabilize the dispersion.[70,71] The pH and salt concentration are also commonly used levers for controlling aggregation.[72,73] Moreover, the barrier to aggregation can be adjusted along a continuum by varying these parameters. Dramatically decreasing the barrier to aggregation can cause formation of fractal-like aggregates.[74] In many instances, a more controlled assembly process is desired, where a minor decrease in the barrier to aggregation drives slower aggregation, but with improved control.[75] It should also be noted that adjusting the conditions of the system may have different effects on AA, AB, and BB interactions, which could allow targeting of AA or BB homoaggregates or AB heteroaggregates.

We are aware of only two examples of heteroaggregation in nonaqueous systems, where NPs were not purposefully charged to drive heteroaggregation. We emphasize nonaqueous systems because we show that adjusting the composition of a solvent mixture is a highly effective means of controlling heteroaggregation. While charging NPs can be useful for self-assembly, we prefer milder conditions, and steric stabilization can be more effective at rendering NPs dispersible in different solvent environments. In one study, oleic acid-stabilized Fe_3O_4 NPs bound to the surfaces of larger SiO_2 NPs over the period of a month and yielded only 30% coverage of the SiO_2 surface.[32] In another study, CdSe and Au NPs stabilized with hydrophobic ligands were deposited onto the surface of much larger, SiO_2-coated Ag nanowires.[37] The extent of coverage was also limited, and heteroaggregation occurred over several weeks. These studies provide useful insights about heteroaggregation, but in both cases, the limited coverage and long assembly time were significant challenges. These are not intrinsic limitations, however, and we show that heteroaggregation can occur quickly and can give dense coatings. The key to achieving this improvement is adjusting the solvent conditions to properly control heteroaggregation, which was not explored in these prior studies.

Controlled assembly of Fe_3O_4-SiO_2-GNRs is achieved by inducing heteroaggregation via mixing of presynthesized Fe_3O_4 NPs and SiO_2-GNRs dispersed in nonpolar (hexanes) and polar (ethanol) solvents, respectively. Fe_3O_4 NPs are deposited onto the surface of SiO_2-GNRs. Although others have produced similar GNR/Fe_3O_4 core/satellite NPs,[6,54−58] major advantages of this method are its simplicity, speed (<10 min), and potential generality. The SiO_2 shell mediates the interaction between the GNR and the Fe_3O_4 NPs, and no additional molecular cross-linker is employed. This heteroaggregation approach can likely be extended to other kinds of SiO_2-coated NPs or surfaces and NPs with hydrophobic ligands. The coatings of Fe_3O_4 NPs allow for manipulation of Fe_3O_4-SiO_2-GNRs with applied magnetic fields.

EXPERIMENTAL SECTION

Experimental methods for synthesizing SiO_2-GNRs,[76,77] Fe_3O_4 NPs,[78] and poly(ethyelene glycol) catechol (PEG-catechol)[79] have already been reported elsewhere. Details for these syntheses are provided in the Supporting Information.

Assembly of Fe_3O_4-SiO_2-GNRs. Hexanes (EMD, ACS, 98.5%) and anhydrous ethanol (Koptec, 99.5%) were used for assembly of Fe_3O_4-SiO_2-GNRs by driving heteroaggregation of Fe_3O_4 NPs and SiO_2-GNRs. The concentration of SiO_2-GNRs was 3.8 mg (measured as mg of Au)/mL of methanol, based on the assumption of 100% yields in the synthesis and purification of GNRs[76] and of SiO_2-GNRs.[77] This assumption is generally valid, because there is no apparent loss of material into the supernatant during centrifugation. An amount of 25 μL of SiO_2-GNRs in methanol was transferred into ethanol by dilution to 15 mL with ethanol. The dispersion was then centrifuged at 8500g (IEC Centra MP4 with 854 rotor) for 10 min and redispersed in 1 mL of ethanol, resulting in a final concentration of 0.095 mg/mL in ethanol. A 2 mL dispersion of Fe_3O_4 NPs in hexanes was prepared with a concentration of 1 mg/mL. These solutions, 1 mL of SiO_2-GNRs in ethanol and 2 mL of Fe_3O_4 NPs in hexanes, were then mixed with rapid stirring, followed by centrifugation at 2500g for 5 min. After removing the supernatant, the sedimented product was

DOI: 10.1021/acs.chemmater.7b03481
Chem. Mater. 2017, 29, 10362−10368

redispersed in hexanes. Fe_3O_4-SiO_2-GNRs can also be dispersed in other weakly polar solvents, such as toluene and tetrahydrofuran (THF). A cylindrical NdFeB permanent magnet (Bunting Magnetics, 1 in. diameter, 0.5 in. long, N35P1000500 for Figure 3a, 0.5 in. diameter, 0.5 in. long, N35P500500 for Figure 3b,c) was then placed next to the side of the glass vial to collect the Fe_3O_4-SiO_2-GNRs, leaving any excess free Fe_3O_4 NPs in the supernatant.

Functionalization of Fe_3O_4-SiO_2-GNRs with PEG-Catechol. Functionalization of Fe_3O_4-SiO_2-GNRs with PEG-catechol was conducted by adapting a method reported for functionalization of Fe_3O_4 NPs.[79] For PEGylation, Fe_3O_4-SiO_2-GNRs were first suspended in toluene by purifying Fe_3O_4-SiO_2-GNRs as described above but redispersing the product in the same volume of toluene instead of hexanes, resulting in the same concentration. The Fe_3O_4-SiO_2-GNRs in toluene were sonicated for 5 min to ensure they were well dispersed. PEG-catechol was dissolved in a small amount of toluene until reaching a final concentration of 0.1 mg/μL. This solution was mixed with the Fe_3O_4-SiO_2-GNRs at ratio of 2 mg of PEG-catechol per mg of SiO_2-GNRs, where the mass of Fe_3O_4 NPs is neglected, and 100% yield as assumed during the heteroaggregation process. The mixture was then heated to 50 °C for 2 h with gentle magnetic stirring. After cooling to room temperature, hexanes was added to drive flocculation, followed by centrifugation at low speed (2500g), removal of the supernatant, and allowing the solvent to completely evaporate under ambient atmosphere. The precipitate was then dispersed in deionized water (Ricca, ACS Reagent grade, ASTM Type I, ASTM Type II) or anhydrous ethanol and briefly sonicated to drive dispersion of PEG-Fe_3O_4-SiO_2-GNRs.

Characterization. Transmission electron microscopy (TEM) was performed using a JEOL 2000FX microscope operated at 200 kV. Optical absorbance spectra were acquired with an Ocean Optics CHEM-USB-VIS-NIR spectrophotometer.

RESULTS AND DISCUSSION

Heteroaggregation was performed using presynthesized CTAB-stabilized GNRs with core dimensions of 94 nm × 24 nm and a 19 nm thick mesoporous SiO_2 coating dispersed in ethanol (Figure 1a) and oleylamine-stabilized Fe_3O_4 NPs with a

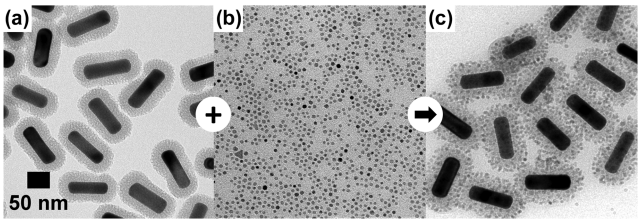

Figure 1. TEM images (common scale bar) of (a) SiO_2-GNRs with 19 nm SiO_2 shells, (b) 7 nm Fe_3O_4 NPs, and (c) Fe_3O_4-SiO_2-GNRs formed by heteroaggregation of Fe_3O_4 NPs onto SiO_2-GNRs.

diameter of 7 nm (Figure 1b) dispersed in hexanes. Under optimized conditions, adding the SiO_2-GNRs in ethanol to the Fe_3O_4 NPs in hexanes yields a uniform coating of Fe_3O_4 NPs on the surface of the SiO_2-GNRs (Figure 1c). Fe_3O_4-SiO_2-GNRs can be assembled and purified by centrifugation in under 10 min. The uniformity of the coating of Fe_3O_4 NPs depends on many variables, including the concentration of Fe_3O_4 NPs and the ethanol to hexanes ratio. For too high concentrations of Fe_3O_4 NPs (>∼10 mg/mL prior to addition to the SiO_2-GNR solution), the Fe_3O_4 NPs undergo homoaggregation before binding to the SiO_2 surface, resulting in large clusters of Fe_3O_4 NPs bound to the surface of SiO_2-GNRs. If too much ethanol is added, the Fe_3O_4 NP coating loses its uniformity, and fractal-shaped aggregates form on the surface of the SiO_2-GNRs or aggregates of Fe_3O_4-SiO_2-GNRs form (unpublished). It is important to add the SiO_2-GNRs to the Fe_3O_4 NPs to avoid homoaggregation of the Fe_3O_4 NPs, which can occur if a small volume of hexanes containing Fe_3O_4 NPs is added to a much larger volume of SiO_2-GNRs in ethanol. The Fe_3O_4-SiO_2-GNR products from heteroaggregation can be purified by centrifugation or magnetic extraction. Fe_3O_4-SiO_2-GNRs disperse well in weakly polar solvents, such as hexanes, toluene, and THF, but do not disperse in ethanol, methanol, or water because the exterior surface of the Fe_3O_4-SiO_2-GNRs is coated with hydrophobic oleylamine ligands.

Mechanism of Heteroaggregation. When Fe_3O_4 NPs dispersed in hexanes are mixed with SiO_2-GNRs dispersed in ethanol under optimized conditions, irreversible heteroaggregation occurs, while avoiding homoaggregation of Fe_3O_4 NPs or SiO_2-GNRs. Under these conditions, the barrier for heteroaggregation is lowered while maintaining the barriers for homoaggregation. As noted above, using a larger proportion of ethanol also reduced the barrier for homoaggregation of Fe_3O_4 NPs, resulting in homoaggregation of Fe_3O_4 NPs. The dependence on the composition of the solvent mixture suggests the energy barrier for heteroaggregation is lower than for homoaggregation of Fe_3O_4 NPs, which may be rationalized by the relatively weak nonpolar interactions between oleylamine-stabilized Fe_3O_4 NPs, in comparison with the stronger interactions with the polar surfaces of SiO_2-GNRs. The large size of the SiO_2-GNRs may also provide additional driving force for heteroaggregation, because the strength of van der Waals interactions increases as the size of the NPs increases. Homoaggregation of SiO_2-GNRs was not observed, which might be attributed to colloidal stability imparted by the SiO_2 shells or because the concentration of SiO_2-GNRs is much lower than that of the Fe_3O_4 NPs.

Optical Properties. Fe_3O_4 NPs absorb light at the blue end of the visible spectrum (Figure 2). This property is appealing for combining with SiO_2-GNRs, because there is minimal spectral overlap between Fe_3O_4 NPs and the LSPR of GNRs. Optical absorbance spectra of Fe_3O_4-SiO_2-GNRs show a redshift of ∼30 nm in the LSPR when the coating of Fe_3O_4

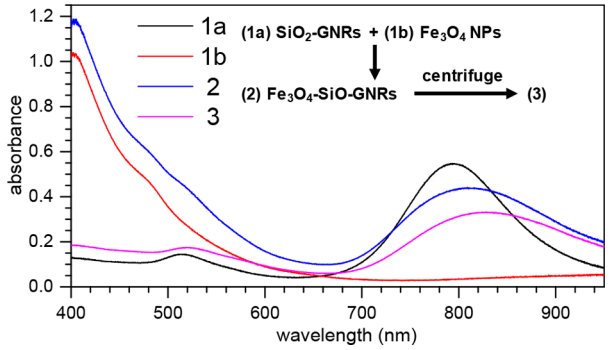

Figure 2. Optical absorbance spectra of the assembly and purification of (1a) SiO_2-GNRs in ethanol and (1b) Fe_3O_4 NPs in hexanes: (2) unpurified Fe_3O_4-SiO_2-GNRs upon mixing and (3) Fe_3O_4-SiO_2-GNRs after centrifugation and redispersion in hexanes. Note: The SiO_2-GNR stock solution was diluted with two volumes of ethanol for acquiring 1a, and the Fe_3O_4 NP stock solution was diluted with half a volume of hexanes for acquiring 1b. These dilutions were chosen to mimic mixing of the stock solutions at the 2:1 hexanes:ethanol volume ratio for heteroaggregation, 2. After centrifugation, the product was redispersed in the same volume of solvent as before purification for acquiring 3.

DOI: 10.1021/acs.chemmater.7b03481
Chem. Mater. 2017, 29, 10362−10368

NPs is attached (Figure 2). This redshift is commonly observed when iron oxide NPs are deposited onto GNRs[12,54,55] and is attributed to the higher index of refraction of Fe_3O_4 (2.42)[80] than that of mesoporous SiO_2 (1.28−1.45).[81] In addition to the redshift, the absorbance broadened and decreased in intensity. Product loss during centrifugation was not observed but could be responsible for at least part of the decrease in intensity. According to previous work, the higher dielectric constant of the Fe_3O_4 NPs can also cause the absorbance to broaden and be reduced in intensity.[54,55]

Magnetic Separation. Fe_3O_4-SiO_2-GNRs exhibit a strong magnetic response. When a permanent magnet is placed next to the dispersion of Fe_3O_4-SiO_2-GNRs, they collect on the wall of the vial next to the magnet (Figure 3a). The sedimented Fe_3O_4-SiO_2-GNRs readily redisperse with mild sonication. For quantitative monitoring of the magnetic extraction process, a permanent magnet was placed next to the bottom of a cuvette containing Fe_3O_4-SiO_2-GNRs (Figure 3c). Optical absorbance spectra were collected every 5 min through the part of the solution at the top of the cuvette, from which Fe_3O_4-SiO_2-GNRs were depleted during magnetic extraction (Figure 3b). After 45 min, 85% of the Fe_3O_4-SiO_2-GNRs were removed from solution. A measurement after 120 min shows that 95% of the Fe_3O_4-SiO_2-GNRs have been removed.

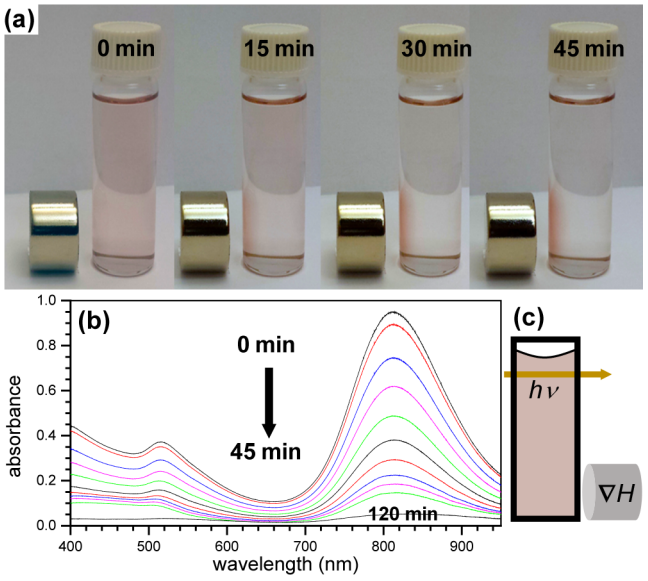

Figure 3. (a) Photos of the magnetic separation process conducted over 45 min. (b) Optical absorbance spectra of Fe_3O_4-SiO_2-GNRs remaining dispersed in hexanes in the top of the cuvette after placing a permanent magnet next to the bottom of the cuvette for magnetic separation. Spectra were collected in 5 min intervals for 45 min, and an additional spectrum was acquired after 120 min. (c) Diagram of the arrangement of the cuvette, magnet, and beam path for measurement of the residual dispersed Fe_3O_4-SiO_2-GNRs that are not pulled to the magnet.

Stability. A sample of Fe_3O_4-SiO_2-GNRs was repeatedly magnetically separated by redispersing the solids captured on the wall of the vial next to the magnet in fresh hexanes and sonicating to investigate the robustness of the coating of Fe_3O_4 NPs in Fe_3O_4-SiO_2-GNRs (Figure 4 and Supporting Information, Figure S1). An optical absorbance spectrum was acquired after each round of magnetic extraction and sonication. The spectra were normalized at 400 nm because

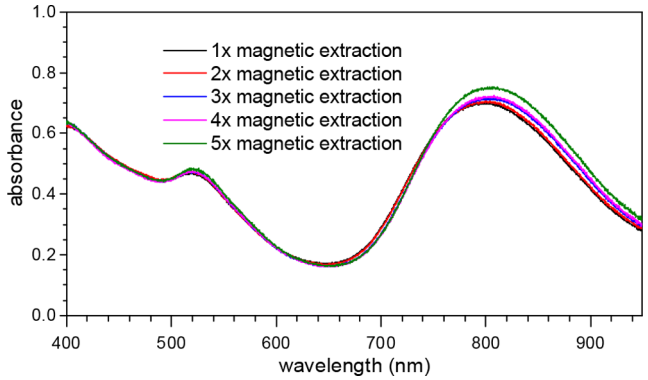

Figure 4. Optical absorbance spectra of Fe_3O_4-SiO_2-GNRs during five rounds of purification through magnetic extraction, normalized at 400 nm. Before acquiring each spectrum, the Fe_3O_4-SiO_2-GNRs were magnetically extracted using a permanent magnet. The supernatant was removed, and the Fe_3O_4-SiO_2-GNRs collected on the wall of the vial next to the magnet were redispersed in a fixed volume of fresh hexanes and sonicated for 5 min.

Fe_3O_4 NPs and GNRs both contribute the absorbance at 400 nm (Figure 2). In the normalized absorbance spectra, the peak for the LSPR begins to broaden and increase in intensity starting after the third extraction and more substantially after the fifth extraction. The increase in peak height can be explained by loss of a small amount of Fe_3O_4 NPs from the surface of the Fe_3O_4-SiO_2-GNRs, because normalization at 400 nm combined with a decrease in the unnormalized absorbance at 400 nm causes an increase in the normalized absorbance at longer wavelengths. The unnormalized spectra also show decreased absorbance after each magnetic extraction step because the NPs adhere to the walls of the glass cuvette (Supporting Information, Figure S1). Broadening of the peak for the LSPR could result from agglomeration of Fe_3O_4-SiO_2-GNRs when some Fe_3O_4 NPs are removed from their surfaces or when some of the oleylamine ligands have been stripped away, because the hydrophobic coatings on the Fe_3O_4 NPs are required for maintaining dispersibility of Fe_3O_4-SiO_2-GNRs in hexanes.

Functionalization for Dispersion in Water. Surface functionalization without removing the Fe_3O_4 NPs from the surface is needed for dispersing Fe_3O_4-SiO_2-GNRs in water for biomedical applications. The Fe_3O_4-SiO_2-GNRs were first transferred into toluene to confer miscibility with PEG-catechol, which was added to displace oleylamine and PEGylate the Fe_3O_4-SiO_2-GNRs, yielding PEG-Fe_3O_4-SiO_2-GNRs. The catechol group binds to the exposed Fe_3O_4 surface, and the PEG moiety provides stability in ethanol and water.[79] PEG-Fe_3O_4-SiO_2-GNRs form an aqueous dispersion that is stable for at least a month. Further experiments would be needed to assess their stability in buffers and biological environments. The optical absorbance spectrum of PEG-Fe_3O_4-SiO_2-GNRs shows neither scattering nor a redshift that would be associated with agglomeration (Figure 5a and Supporting Information, Figure S2). Rather, the absorbance spectrum maintains the prominent absorption band of Fe_3O_4-SiO_2-GNRs prior to PEGylation and shows no sign of detachment of Fe_3O_4 NPs. There is a blueshift in the LSPR by ∼15 nm, which can be attributed to differences in the refractive index of toluene and water.[82] TEM of the PEG-Fe_3O_4-SiO_2-GNRs confirms that surface functionalization can be conducted without displacing the coating of Fe_3O_4 NPs (Figure 5c).

DOI: 10.1021/acs.chemmater.7b03481
Chem. Mater. 2017, 29, 10362−10368

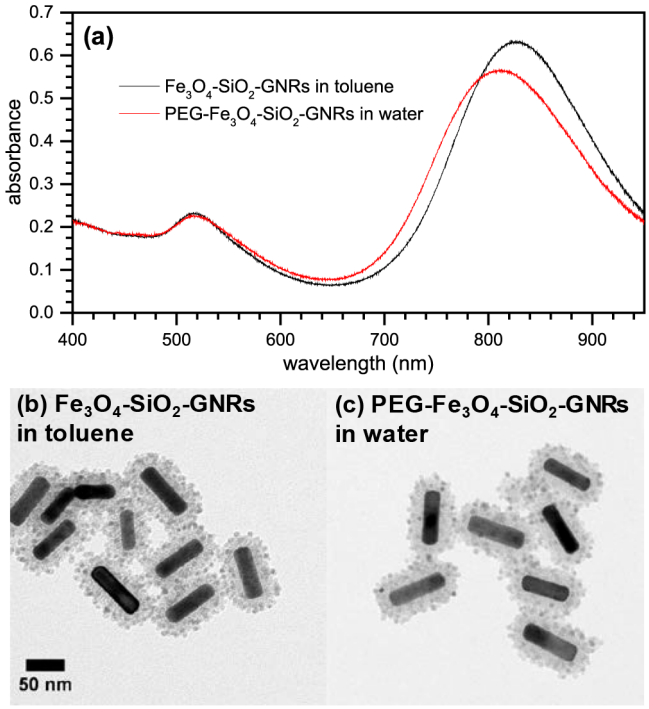

Figure 5. (a) Optical absorbance spectra, normalized at 400 nm, and TEM (common scale bar) of (b) Fe_3O_4-SiO_2-GNRs in toluene and (c) PEG-Fe_3O_4-SiO_2-GNRs in water.

CONCLUSIONS

By employing the well-known property of NPs stabilized by hydrophobic ligands to aggregate when exposed to polar nonsolvents, we have developed a method for quickly inducing heteroaggregation of Fe_3O_4 NPs onto the surface of SiO_2-GNRs, resulting in Fe_3O_4-SiO_2-GNRs with a core/satellite morphology. By controlling the solvent polarity, uniform coatings of Fe_3O_4 NPs can be deposited onto the surface of SiO_2-GNRs within a few minutes of mixing and without requiring an additional cross-linker. This method is simple and fast because it uses presynthesized NPs, which allows independent control over the synthesis of the core and satellite NPs. Fe_3O_4-SiO_2-GNRs maintain the LSPR of the GNRs in the core and also exhibit strong responses to permanent magnets, thus allowing for magnetic manipulation and separations. Fe_3O_4-SiO_2-GNRs disperse in nonpolar and weakly polar solvents, including hexanes, toluene, and THF. Surface functionalization with PEG-catechol renders them dispersible in water. Since many types of NPs are synthesized using hydrophobic ligands and methods for overcoating NPs with SiO_2 are well established, this technique could potentially be used to assemble a wide variety of core/satellite NPs. We anticipate this demonstration of a fast, nonaqueous heteroaggregation process will stimulate further work to apply heteroaggregation in other nonaqueous systems and to further investigate the mechanisms of heteroaggregation.

ASSOCIATED CONTENT

Supporting Information

The Supporting Information is available free of charge on the ACS Publications website at DOI: 10.1021/acs.chemmater.7b03481.

Methods for synthesizing and purifying SiO_2-GNRs, Fe_3O_4 NPs, and PEG-catechol and unnormalized optical absorbance spectra (PDF)

Video of heteroaggregation process and magnetic extraction (MPG)

AUTHOR INFORMATION

Corresponding Author

*(J.B.T.) E-mail: jbtracy@ncsu.edu.

ORCID

Joseph B. Tracy: 0000-0002-3358-3703

Notes

The authors declare no competing financial interest.

ACKNOWLEDGMENTS

This research was supported by the National Science Foundation (Research Triangle MRSEC, DMR-1121107, DMR-1056653, and CBET-1605699). We thank Sumeet Mishra for training in the synthesis of Fe_3O_4 NPs and Allison McGinnis for conducting related experiments that contributed to the design of this study. This work was performed in part at the Analytical Instrumentation Facility (AIF) at North Carolina State University, which is supported by the State of North Carolina and the National Science Foundation (ECCS-1542015). The AIF is a member of the North Carolina Research Triangle Nanotechnology Network (RTNN), a site in the National Nanotechnology Coordinated Infrastructure (NNCI).

REFERENCES

(1) Buck, M. R.; Schaak, R. E. Emerging Strategies for the Total Synthesis of Inorganic Nanostructures. *Angew. Chem., Int. Ed.* **2013**, *52*, 6154−6178.

(2) Sahay, R.; Reddy, V. J.; Ramakrishna, S. Synthesis and Applications of Multifunctional Composite Nanomaterials. *Int. J. Mech. Mater. Eng.* **2014**, *9*, 25.

(3) Liu, X.; Iocozzia, J.; Wang, Y.; Cui, X.; Chen, Y.; Zhao, S.; Li, Z.; Lin, Z. Noble Metal-Metal Oxide Nanohybrids with Tailored Nanostructures for Efficient Solar Energy Conversion, Photocatalysis and Environmental Remediation. *Energy Environ. Sci.* **2017**, *10*, 402−434.

(4) Nguyen, T.-D.; Tran, T.-H. Multicomponent Nanoarchitectures for the Design of Optical Sensing and Diagnostic Tools. *RSC Adv.* **2014**, *4*, 916−942.

(5) Lin, X.-M.; Samia, A. C. S. Synthesis, Assembly and Physical Properties of Magnetic Nanoparticles. *J. Magn. Magn. Mater.* **2006**, *305*, 100−109.

(6) Gole, A.; Stone, J. W.; Gemmill, W. R.; zur Loye, H.-C.; Murphy, C. J. Iron Oxide Coated Gold Nanorods: Synthesis, Characterization, and Magnetic Manipulation. *Langmuir* **2008**, *24*, 6232−6237.

(7) Shevchenko, E. V.; Bodnarchuk, M. I.; Kovalenko, M. V.; Talapin, D. V.; Smith, R. K.; Aloni, S.; Heiss, W.; Alivisatos, A. P. Gold/Iron Oxide Core/Hollow-Shell Nanoparticles. *Adv. Mater.* **2008**, *20*, 4323−4329.

(8) Wei, Y.; Klajn, R.; Pinchuk, A. O.; Grzybowski, B. A. Synthesis, Shape Control, and Optical Properties of Hybrid Au/Fe_3O_4 "Nanoflowers. *Small* **2008**, *4*, 1635−1639.

(9) Sheldon, M. T.; Trudeau, P.-E.; Mokari, T.; Wang, L.-W.; Alivisatos, A. P. Enhanced Semiconductor Nanocrystal Conductance via Solution Grown Contacts. *Nano Lett.* **2009**, *9*, 3676−3682.

(10) Carbone, L.; Cozzoli, P. D. Colloidal Heterostructured Nanocrystals: Synthesis and Growth Mechanisms. *Nano Today* **2010**, *5*, 449−493.

DOI: 10.1021/acs.chemmater.7b03481
Chem. Mater. 2017, 29, 10362−10368

(11) Shore, M. S.; Wang, J.; Johnston-Peck, A. C.; Oldenburg, A. L.; Tracy, J. B. Synthesis of Au(Core)/Ag(Shell) Nanoparticles and their Conversion to AuAg Alloy Nanoparticles. *Small* **2011**, *7*, 230−234.
(12) Zhai, Y.; Han, L.; Wang, P.; Li, G.; Ren, W.; Liu, L.; Wang, E.; Dong, S. Superparamagnetic Plasmonic Nanohybrids: Shape-Controlled Synthesis, TEM-Induced Structure Evolution, and Efficient Sunlight-Driven Inactivation of Bacteria. *ACS Nano* **2011**, *5*, 8562−8570.
(13) Hill, L. J.; Bull, M. M.; Sung, Y.; Simmonds, A. G.; Dirlam, P. T.; Richey, N. E.; DeRosa, S. E.; Shim, I.-B.; Guin, D.; Costanzo, P. J.; Pinna, N.; Willinger, M.-G.; Vogel, W.; Char, K.; Pyun, J. Directing the Deposition of Ferromagnetic Cobalt onto Pt-Tipped CdSe@CdS Nanorods: Synthetic and Mechanistic Insights. *ACS Nano* **2012**, *6*, 8632−8645.
(14) Xu, Y.; Lian, J.; Mishra, N.; Chan, Y. Multifunctional Semiconductor Nanoheterostructures via Site-Selective Silica Encapsulation. *Small* **2013**, *9*, 1908−1915.
(15) Gao, C.; Goebl, J.; Yin, Y. Seeded Growth Route to Noble Metal Nanostructures. *J. Mater. Chem. C* **2013**, *1*, 3898−3909.
(16) Banin, U.; Ben-Shahar, Y.; Vinokurov, K. Hybrid Semiconductor−Metal Nanoparticles: From Architecture to Function. *Chem. Mater.* **2014**, *26*, 97−110.
(17) Zhou, H.; Kim, J.-P.; Bahng, J. H.; Kotov, N. A.; Lee, J. Self-Assembly Mechanism of Spiky Magnetoplasmonic Supraparticles. *Adv. Funct. Mater.* **2014**, *24*, 1439−1448.
(18) Straney, P. J.; Marbella, L. E.; Andolina, C. M.; Nuhfer, N. T.; Millstone, J. E. Decoupling Mechanisms of Platinum Deposition on Colloidal Gold Nanoparticle Substrates. *J. Am. Chem. Soc.* **2014**, *136*, 7873−7876.
(19) Yu, S.; Hachtel, J. A.; Chisholm, M. F.; Pantelides, S. T.; Laromaine, A.; Roig, A. Magnetic Gold Nanotriangles by Microwave-Assisted Polyol Synthesis. *Nanoscale* **2015**, *7*, 14039−14046.
(20) Weiner, R. G.; Kunz, M. R.; Skrabalak, S. E. Seeding a New Kind of Garden: Synthesis of Architecturally Defined Multimetallic Nanostructures by Seed-Mediated Co-Reduction. *Acc. Chem. Res.* **2015**, *48*, 2688−2695.
(21) Hernández-Pagán, E. A.; Leach, A. D. P.; Rhodes, J. M.; Sarkar, S.; Macdonald, J. E. A Synthetic Exploration of Metal−Semiconductor Hybrid Particles of $CuInS_2$. *Chem. Mater.* **2015**, *27*, 7969−7976.
(22) Pavlopoulos, N. G.; Dubose, J. T.; Pinna, N.; Willinger, M.-G.; Char, K.; Pyun, J. Synthesis and Assembly of Dipolar Heterostructured Tetrapods: Colloidal Polymers with "Giant *tert*-butyl" Groups. *Angew. Chem., Int. Ed.* **2016**, *55*, 1787−1791.
(23) Pang, B.; Zhao, Y.; Luehmann, H.; Yang, X.; Detering, L.; You, M.; Zhang, C.; Zhang, L.; Li, Z.-Y.; Ren, Q.; Liu, Y.; Xia, Y. ^{64}Cu-Doped PdCu@Au Tripods: A Multifunctional Nanomaterial for Positron Emission Tomography and Image-Guided Photothermal Cancer Treatment. *ACS Nano* **2016**, *10*, 3121−3131.
(24) Nakibli, Y.; Amirav, L. Selective Growth of Ni Tips on Nanorod Photocatalysts. *Chem. Mater.* **2016**, *28*, 4524−4527.
(25) Gilroy, K. D.; Ruditskiy, A.; Peng, H.-C.; Qin, D.; Xia, Y. Bimetallic Nanocrystals: Syntheses, Properties, and Applications. *Chem. Rev.* **2016**, *116*, 10414−10472.
(26) Su, X.; Fu, B.; Yuan, J. Gold Nanocluster-Coated Gold Nanorods for Simultaneously Enhanced Photothermal Performance and Stability. *Mater. Lett.* **2017**, *188*, 111−114.
(27) Li, Y.; Zhao, J.; You, W.; Cheng, D.; Ni, W. Gold Nanorod@Iron Oxide Core-Shell Heterostructures: Synthesis, Characterization, and Photocatalytic Performance. *Nanoscale* **2017**, *9*, 3925−3933.
(28) Marusak, K. E.; Johnston-Peck, A. C.; Wu, W.-C.; Anderson, B. D.; Tracy, J. B. Size and Composition Control of CoNi Nanoparticles and Their Conversion into Phosphides. *Chem. Mater.* **2017**, *29*, 2739−2747.
(29) Reguera, J.; Jiménez de Aberasturi, D.; Henriksen-Lacey, M.; Langer, J.; Espinosa, A.; Szczupak, B.; Wilhelm, C.; Liz-Marzán, L. M. Janus Plasmonic-Magnetic Gold-Iron Oxide Nanoparticles as Contrast Agents for Multimodal Imaging. *Nanoscale* **2017**, *9*, 9467−9480.
(30) Zhan, W.; Wang, J.; Wang, H.; Zhang, J.; Liu, X.; Zhang, P.; Chi, M.; Guo, Y.; Guo, Y.; Lu, G.; Sun, S.; Dai, S.; Zhu, H. Crystal Structural Effect of AuCu Alloy Nanoparticles on Catalytic CO Oxidation. *J. Am. Chem. Soc.* **2017**, *139*, 8846−8854.
(31) Chen, P.-C.; Liu, X.; Hedrick, J. L.; Xie, Z.; Wang, S.; Lin, Q.-Y.; Hersam, M. C.; Dravid, V. P.; Mirkin, C. A. Polyelemental Nanoparticle Libraries. *Science* **2016**, *352*, 1565−1569.
(32) van Ewijk, G. A.; Philipse, A. P. Anomalous Attraction between Colloidal Magnetite and Silica Spheres in Apolar Solvents. *Langmuir* **2001**, *17*, 7204−7209.
(33) Kalsin, A. M.; Pinchuk, A. O.; Smoukov, S. K.; Paszewski, M.; Schatz, G. C.; Grzybowski, B. A. Electrostatic Aggregation and Formation of Core−Shell Suprastructures in Binary Mixtures of Charged Metal Nanoparticles. *Nano Lett.* **2006**, *6*, 1896−1903.
(34) Yeap, S. P.; Toh, P. Y.; Ahmad, A. L.; Low, S. C.; Majetich, S. A.; Lim, J. Colloidal Stability and Magnetophoresis of Gold-Coated Iron Oxide Nanorods in Biological Media. *J. Phys. Chem. C* **2012**, *116*, 22561−22569.
(35) Caputo, G.; Pinna, N. Nanoparticle Self-Assembly Using π-π Interactions. *J. Mater. Chem. A* **2013**, *1*, 2370−2378.
(36) Essinger-Hileman, E. R.; Popczun, E. J.; Schaak, R. E. Magnetic Separation of Colloidal Nanoparticle Mixtures Using a Material Specific Peptide. *Chem. Commun.* **2013**, *49*, 5471−5473.
(37) Pita, I. A.; Singh, S.; Silien, C.; Ryan, K. M.; Liu, N. Heteroaggregation Assisted Wet Synthesis of Core-Shell Silver-Silica-Cadmium Selenide Nanowires. *Nanoscale* **2016**, *8*, 1200−1209.
(38) Kister, T.; Mravlak, M.; Schilling, T.; Kraus, T. Pressure-Controlled Formation of Crystalline, Janus, and Core-Shell Supraparticles. *Nanoscale* **2016**, *8*, 13377−13384.
(39) Lu, Z.; Qin, Y.; Fang, J.; Sun, J.; Li, J.; Liu, F.; Yang, W. Monodisperse Magnetizable Silica Composite Particles from Heteroaggregate of Carboxylic Polystyrene Latex and Fe_3O_4 Nanoparticles. *Nanotechnology* **2008**, *19*, 055602.
(40) Munshi, A. M.; Ho, D.; Saunders, M.; Agarwal, V.; Raston, C. L.; Iyer, K. S. Influence of Aspect Ratio of Magnetite Coated Gold Nanorods in Hydrogen Peroxide Sensing. Sens. *Sens. Actuators, B* **2016**, *235*, 492−497.
(41) Liu, N.; Prall, B. S.; Klimov, V. I. Hybrid Gold/Silica/Nanocrystal-Quantum-Dot Superstructures: Synthesis and Analysis of Semiconductor-Metal Interactions. *J. Am. Chem. Soc.* **2006**, *128*, 15362−15363.
(42) Guo, S.; Dong, S.; Wang, E. A General Route to Construct Diverse Multifunctional Fe_3O_4/Metal Hybrid Nanostructures. *Chem. - Eur. J.* **2009**, *15*, 2416−2424.
(43) Lu, Z.; Gao, C.; Zhang, Q.; Chi, M.; Howe, J. Y.; Yin, Y. Direct Assembly of Hydrophobic Nanoparticles to Multifunctional Structures. *Nano Lett.* **2011**, *11*, 3404−3412.
(44) Yin, N.; Jiang, T.; Yu, J.; He, J.; Li, X.; Huang, Q.; Liu, L.; Xu, X.; Zhu, L. Study of Gold Nanostar@SiO_2@CdTeS Quantum Dots@SiO_2 with Enhanced-Fluorescence and Photothermal Therapy Multifunctional Cell Nanoprobe. *J. Nanopart. Res.* **2014**, *16*, 2306.
(45) Jeoung, E.; Yeh, Y.-C.; Nelson, T.; Kushida, T.; Wang, L.-S.; Mout, R.; Li, X.; Saha, K.; Gupta, A.; Tonga, G. Y.; Lannutti, J. J.; Rotello, V. M. Fabrication of Functional Nanofibers Through Post-Nanoparticle Functionalization. *Macromol. Rapid Commun.* **2015**, *36*, 678−683.
(46) Ertem, E.; Murillo-Cremaes, N.; Carney, R. P.; Laromaine, A.; Janecek, E.-R.; Roig, A.; Stellacci, F. A Silica-Based Magnetic Platform Decorated with Mixed Ligand Gold Nanoparticles: A Recyclable Catalyst for Esterification Reactions. *Chem. Commun.* **2016**, *52*, 5573−5576.
(47) Höller, R. P. M.; Dulle, M.; Thomä, S.; Mayer, M.; Steiner, A. M.; Förster, S.; Fery, A.; Kuttner, C.; Chanana, M. Protein-Assisted Assembly of Modular 3D Plasmonic Raspberry-Like Core/Satellite Nanoclusters: Correlation of Structure and Optical Properties. *ACS Nano* **2016**, *10*, 5740−5750.
(48) Zhang, M.; Magagnosc, D. J.; Liberal, I.; Yu, Y.; Yun, H.; Yang, H.; Wu, Y.; Guo, J.; Chen, W.; Shin, Y. J.; Stein, A.; Kikkawa, J. M.; Engheta, N.; Gianola, D. S.; Murray, C. B.; Kagan, C. R. High-Strength Magnetically Switchable Plasmonic Nanorods Assembled from a Binary Nanocrystal Mixture. *Nat. Nanotechnol.* **2017**, *12*, 228−232.

DOI: 10.1021/acs.chemmater.7b03481
Chem. Mater. 2017, 29, 10362−10368

(49) Cha, J.; Cui, P.; Lee, J.-K. A Simple Method to Synthesize Multifunctional Silica Nanocomposites, NPs@SiO_2, Using Polyvinylpyrrolidone (PVP) as a Mediator. *J. Mater. Chem.* **2010**, *20*, 5533−5537.
(50) Chan, Y.; Zimmer, J. P.; Stroh, M.; Steckel, J. S.; Jain, R. K.; Bawendi, M. G. Incorporation of Luminescent Nanocrystals into Monodisperse Core-Shell Silica Microspheres. *Adv. Mater.* **2004**, *16*, 2092−2097.
(51) Yi, D. K.; Selvan, S. T.; Lee, S. S.; Papaefthymiou, G. C.; Kundaliya, D.; Ying, J. Y. Silica-Coated Nanocomposites of Magnetic Nanoparticles and Quantum Dots. *J. Am. Chem. Soc.* **2005**, *127*, 4990−4991.
(52) Insin, N.; Tracy, J. B.; Lee, H.; Zimmer, J. P.; Westervelt, R. M.; Bawendi, M. G. Incorporation of Iron Oxide Nanoparticles and Quantum Dots into Silica Microspheres. *ACS Nano* **2008**, *2*, 197−202.
(53) Chen, O.; Riedemann, L.; Etoc, F.; Herrmann, H.; Coppey, M.; Barch, M.; Farrar, C. T.; Zhao, J.; Bruns, O. T.; Wei, H.; Guo, P.; Cui, J.; Jensen, R.; Chen, Y.; Harris, D. K.; Cordero, J. M.; Wang, Z.; Jasanoff, A.; Fukumura, D.; Reimer, R.; Dahan, M.; Jain, R. K.; Bawendi, M. G. Magneto-Fluorescent Core-Shell Supernanoparticles. *Nat. Commun.* **2014**, *5*, 5093.
(54) Truby, R. L.; Emelianov, S. Y.; Homan, K. A. Ligand-Mediated Self-Assembly of Hybrid Plasmonic and Superparamagnetic Nanostructures. *Langmuir* **2013**, *29*, 2465−2470.
(55) Wang, C.; Chen, J.; Talavage, T.; Irudayaraj, J. Gold Nanorod/Fe_3O_4 Nanoparticle "Nano-Pearl-Necklaces" for Simultaneous Targeting, Dual-Mode Imaging, and Photothermal Ablation of Cancer Cells. *Angew. Chem., Int. Ed.* **2009**, *48*, 2759−2763.
(56) Basiruddin, S. K.; Maity, A. R.; Saha, A.; Jana, N. R. Gold-Nanorod-Based Hybrid Cellular Probe with Multifunctional Properties. *J. Phys. Chem. C* **2011**, *115*, 19612−19620.
(57) Ramasamy, M.; Lee, S. S.; Yi, D. K.; Kim, K. Magnetic, Optical Gold Nanorods for Recyclable Photothermal Ablation of Bacteria. *J. Mater. Chem. B* **2014**, *2*, 981−988.
(58) Zhang, H.; Sun, Y.; Gao, S.; Zhang, H.; Zhang, J.; Bai, Y.; Song, D. Studies of Gold Nanorod-Iron Oxide Nanohybrids for Immunoassay Based on SPR Biosensor. *Talanta* **2014**, *125*, 29−35.
(59) Fan, Z.; Tebbe, M.; Fery, A.; Agarwal, S.; Greiner, A. Assembly of Gold Nanoparticles on Gold Nanorods Using Functionalized Poly(N-isopropylacrylamide) as Polymeric "Glue. *Part. Part. Syst. Charact.* **2016**, *33*, 698−702.
(60) Wu, X.; Gao, F.; Xu, L.; Kuang, H.; Wang, L.; Xu, C. A Fluorescence Active Gold Nanorod-Quantum Dot Core-Satellite Nanostructure for Sub-Attomolar Tumor Marker Biosensing. *RSC Adv.* **2015**, *5*, 97898−97902.
(61) Raeesi, V.; Chou, L. Y. T.; Chan, W. C. W. Tuning the Drug Loading and Release of DNA-Assembled Gold-Nanorod Superstructures. *Adv. Mater.* **2016**, *28*, 8511−8518.
(62) Hore, M. J. A.; Ye, X.; Ford, J.; Gao, Y.; Fei, J.; Wu, Q.; Rowan, S. J.; Composto, R. J.; Murray, C. B.; Hammouda, B. Probing the Structure, Composition, and Spatial Distribution of Ligands on Gold Nanorods. *Nano Lett.* **2015**, *15*, 5730−5738.
(63) Vigderman, L.; Khanal, B. P.; Zubarev, E. R. Functional Gold Nanorods: Synthesis, Self-Assembly, and Sensing Applications. *Adv. Mater.* **2012**, *24*, 4811−4841.
(64) Verwey, E. J. W. Theory of the Stability of Lyophobic Colloids. *J. Phys. Colloid Chem.* **1947**, *51*, 631−636.
(65) Derjaguin, B.; Landau, L. Theory of the Stability of Strongly Charged Lyophobic Sols and of the Adhesion of Strongly Charged Particles in Solutions of Electrolytes. *Prog. Surf. Sci.* **1993**, *43*, 30−59.
(66) Pugh, R. J. Selective Coagulation of Colloidal Mineral Particles. In *Colloid Chemistry in Mineral Processing*; Elsevier: 1992; Vol. *12*, pp 268−271.
(67) Wang, H.; Adeleye, A. S.; Huang, Y.; Li, F.; Keller, A. A. Heteroaggregation of Nanoparticles with Biocolloids and Geocolloids. *Adv. Colloid Interface Sci.* **2015**, *226*, 24−36.
(68) Stolarczyk, J. K.; Deak, A.; Brougham, D. F. Nanoparticle Clusters: Assembly and Control Over Internal Order, Current Capabilities, and Future Potential. *Adv. Mater.* **2016**, *28*, 5400−5424.
(69) Snoswell, D. R. E.; Duan, J.; Fornasiero, D.; Ralston, J. The Selective Aggregation and Separation of Titania from a Mixed Suspension of Silica and Titania. *Int. J. Miner. Process.* **2005**, *78*, 1−10.
(70) Dutta, N.; Egorov, S.; Green, D. Quantification of Nanoparticle Interactions in Pure Solvents and a Concentrated PDMS Solution as a Function of Solvent Quality. *Langmuir* **2013**, *29*, 9991−10000.
(71) Kislenko, S. A.; Kislenko, V. A.; Razumov, V. F. The Effects of a Solvent and a Ligand Shell on Interaction of CdSe Quantum Dots: Molecular Dynamics Simulation. *Colloid J.* **2015**, *77*, 727−732.
(72) Shen, C.; Li, B.; Huang, Y.; Jin, Y. Kinetics of Coupled Primary- and Secondary-Minimum Deposition of Colloids under Unfavorable Chemical Conditions. *Environ. Sci. Technol.* **2007**, *41*, 6976−6982.
(73) Dušak, P.; Mertelj, A.; Kralj, S.; Makovec, D. Controlled Heteroaggregation of Two Types of Nanoparticles in an Aqueous Suspension. *J. Colloid Interface Sci.* **2015**, *438*, 235−243.
(74) Asnaghi, D.; Carpineti, M.; Giglio, M.; Sozzi, M. Coagulation Kinetics and Aggregate Morphology in the Intermediate Regimes Between Diffusion-Limited and Reaction-Limited Cluster Aggregation. *Phys. Rev. A: At., Mol., Opt. Phys.* **1992**, *45*, 1018−1023.
(75) Lin, M. Y.; Lindsay, H. M.; Weitz, D. A.; Ball, R. C.; Klein, R.; Meakin, P. Universal Reaction-Limited Colloid Aggregation. *Phys. Rev. A: At., Mol., Opt. Phys.* **1990**, *41*, 2005−2020.
(76) Kozek, K. A.; Kozek, K. M.; Wu, W.-C.; Mishra, S. R.; Tracy, J. B. Large-Scale Synthesis of Gold Nanorods through Continuous Secondary Growth. *Chem. Mater.* **2013**, *25*, 4537−4544.
(77) Wu, W.-C.; Tracy, J. B. Large-Scale Silica Overcoating of Gold Nanorods with Tunable Shell Thicknesses. *Chem. Mater.* **2015**, *27*, 2888−2894.
(78) Xu, Z.; Shen, C.; Hou, Y.; Gao, H.; Sun, S. Oleylamine as Both Reducing Agent and Stabilizer in a Facile Synthesis of Magnetite Nanoparticles. *Chem. Mater.* **2009**, *21*, 1778−1780.
(79) Li, Q.; Barrett, D. G.; Messersmith, P. B.; Holten-Andersen, N. Controlling Hydrogel Mechanics via Bio-Inspired Polymer-Nanoparticle Bond Dynamics. *ACS Nano* **2016**, *10*, 1317−1324.
(80) Patnaik, P. *Handbook of Inorganic Chemicals*; McGraw-Hill: New York, 2003.
(81) Brinker, C. J.; Scherer, G. W. *Sol-Gel Science: The Physics and Chemistry of Sol-Gel Processing*; Academic Press: Boston, 1990.
(82) Chen, H.; Kou, X.; Yang, Z.; Ni, W.; Wang, J. Shape- and Size-Dependent Refractive Index Sensitivity of Gold Nanoparticles. *Langmuir* **2008**, *24*, 5233−5237.

DOI: 10.1021/acs.chemmater.7b03481
Chem. Mater. 2017, 29, 10362−10368